# Laser Annealing of Amorphous Ni-Ti Shape Memory Alloy Thin Films

Xi Wang, Zhenyu Xue, Joost J. Vlassak
Division of Engineering and Applied Sciences, Harvard University, Cambridge, MA, U.S.A.

Yves Bellouard
Micro- & Nano-Scale Engineering, Mechanical Engineering, Eindhoven University of Technology, Eindhoven, The Netherlands

## Introduction

Shape memory alloy (SMA) thin films, especially those based on Ni-Ti, have received considerable attention since it was demonstrated that they can undergo a nearly perfect shape memory effect [1-7]. When SMA films are used as actuators in MEMS devices, biasing springs are generally needed to restore the initial state in order to achieve a two-way shape memory effect. As a result, use of SMA actuator in MEMS has been limited mainly to bimorph-like mechanisms. Recently, laser annealing of shape memory alloys (LASMA) emerged as a promising approach for the fabrication of planar mechanisms [8,12]. This technique has the advantage that shape memory properties can be spatially distributed: material crystallized by laser irradiation has shape memory properties and can be used as an actuator, while untransformed material is passive and provides a restoring force. In this paper, we present the results of an experimental study of the laser annealing process for NiTi thin films, along with a computational model.

## Experiments

NiTi thin films with a thickness of approximately 1.5 μm were prepared by co-sputtering a NiTi alloy target and an elemental Ti target. The substrate consisted of 1mm thick fused quartz. The back-ground pressure of the deposition chamber was less than $5.0 \times 10^{-8}$ Torr and the Ar working pressure was 1.5 mTorr. The nominal target-substrate distance was 100 mm; the deposition rate was approximately 20 nm/min. In order to get a uniform film thickness and composition, the substrates were rotated at a speed of 20 RPM. The composition of the films was measured to be $50.5 \pm 0.2$ at. %Ti by means of electron microprobe analysis (EMPA). The as-deposited films were amorphous as confirmed by X-ray diffraction.

In the laser annealing process, samples were annealed by scanning a laser beam over the surface of the films. A fiber-injected CW near-IR laser diode (coherent/925nm) was used to obtain the results presented in this study. The laser beam had a Gaussian power distribution and a diameter of approximately 0.9mm. The specimen was mounted on a platform capable of planar translational and rotational motions with micron resolution. In the experiment, the laser power was varied from 5 to 9.4 W; the scan speed was varied from 1 to 8 mm/s. All scans were performed in air in a thermally stabilized environment. During laser annealing a thin oxide layer was formed on top of the NiTi film. As we will show later in this paper, this oxide plays an important role in the laser annealing process.

## Experimental results

The laser beam was scanned across the film surface in a straight-line pattern. The annealed section of the film was then investigated using optical microscopy. As shown in Fig. 1, the annealed area is rough and shows surface relief in contrast to the shiny unannealed area. The width of the annealed line is a few hundred microns. The structure of the annealed films was investigated systematically as a function of laser power density and scan speed

using X-ray diffraction (XRD) and transmission electron microscopy (TEM); the results are summarized in Fig. 2. At a given scan speed, the film transitions from amorphous to partially

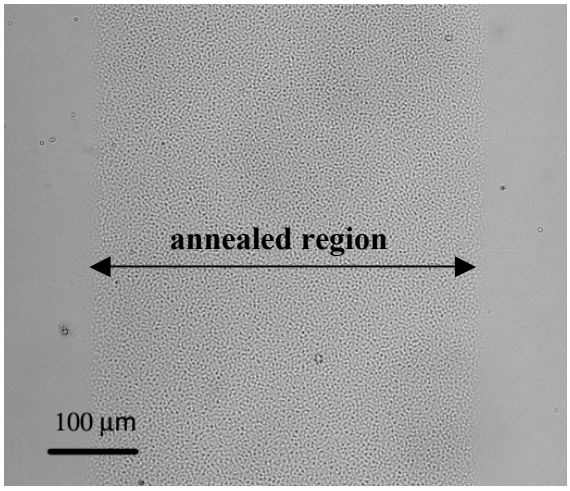


*Figure 1: Optical micrograph of film surface after laser annealing.*

crystalline (crystallites embedded in an amorphous matrix) to eventually fully crystalline (an area of polycrystalline film) as the laser power is increased. If the laser power density is too high, film and substrate crack due to thermal shock. Figure 3 shows the width of the crystalline region as a function of laser power density and scan speed. The width increases with increasing laser power and decreasing scan speed.

In order to get a strong enough signal for the XRD measurements, XRD samples were prepared by scanning the laser over the surface in an array of parallel lines. Figure 4 shows a typical room temperature XRD spectrum of such a multiple-line sample. After laser annealing, the material in the crystalline regions has transformed to martensite demonstrating that shape memory properties can

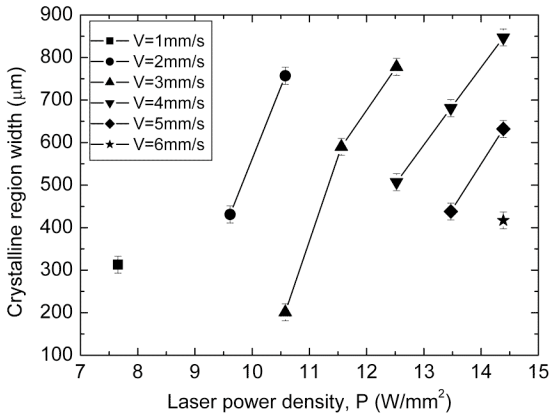


*Figure 3: Width of crystallized region as a function of laser power density and scan speed.*

indeed be introduced using laser annealing. Some R-phase and untransformed parent phase are also present in the film at room temperature.No precipitates were observed in the laser-annealed films because of the short annealing times. The presence of the R-phase and the untransformed $B_2$ phase may be related to the formation of a Ni-rich layer immediately below the surface oxide [9]. TEM specimens were prepared by cutting 3 mm diameter discs from samples that consisted of a single-line scan. The discs were dimpled and the area of interest was thinned to electron transparency by ion beam milling with a 4 kV argon beam. The

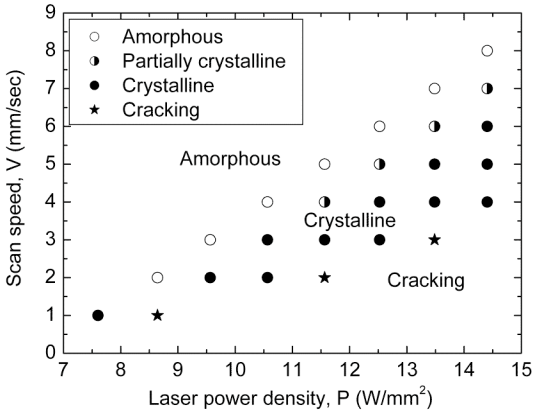


*Figure 2: Crystallization behavior of NiTi films as a function of laser power density and scan*

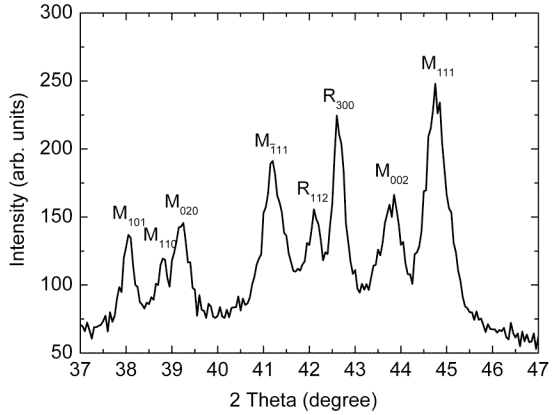


*Figure 4: Room temperature X-ray diffraction spectrum for a sample with multiple-line scan.*

TEM micrograph in Fig. 5 shows a typical microstructure close to the center of the laser trace. Most grains are 1-1.5 μm in diameter although there are a few grains as small as 0.3 μm.

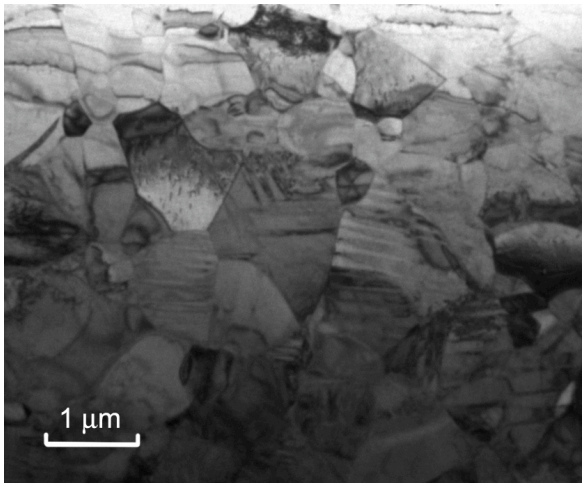


*Figure 5: TEM micrograph of the microstructure close to the center the laser trace.*

**FEM simulation**

The temperature distribution during the laser annealing process was calculated using a fully three-dimensional thermal model. The temperature distribution depends on the incident energy absorbed by the film. If the laser beam moves at a velocity $v$ in the x-direction, the absorbed energy is given by:

$$I = \frac{P(1-R)}{\pi r^2} \exp\left( -\left( \frac{x-vt}{r} \right)^2 - \left( \frac{y}{r} \right)^2 \right), \qquad (1)$$

where $r$ is the Gaussian ($1/e$) radius of the intensity, $P$ is the total incident power, and $R$ is the coefficient of reflection of the irradiated material. The Gaussian nature of the intensity profile of the laser was confirmed by a direct measurement of the laser intensity profile.

A commercial finite element package, ABAQUS®, was used for the simulations. The geometry of the model is illustrated schematically in Fig. 6. The thin film was simulated using 4-node quadrilateral shell heat transfer elements with five Simpson integration points through the shell thickness; the substrate was modeled using 8-node linear brick heat transfer elements. Because of the mirror symmetry along x-axis, only one half of the system was modeled. The surface elements were subjected to a time-dependent heat flux as described by Eq. (1). The heat loss to the ambient through the top and bottom surface was assumed to be negligible, as was the enthalpy of crystallization of the NiTi. The thermal properties of the fused quartz substrates were temperature-dependent and were taken from reference [10]. The thermal properties of the NiTi film were assumed to be constant and equal to the room temperature values. This assumption had only a small effect on the temperature distribution because the temperature of the film is dictated mainly by the temperature and thermal properties of the underlying substrate.

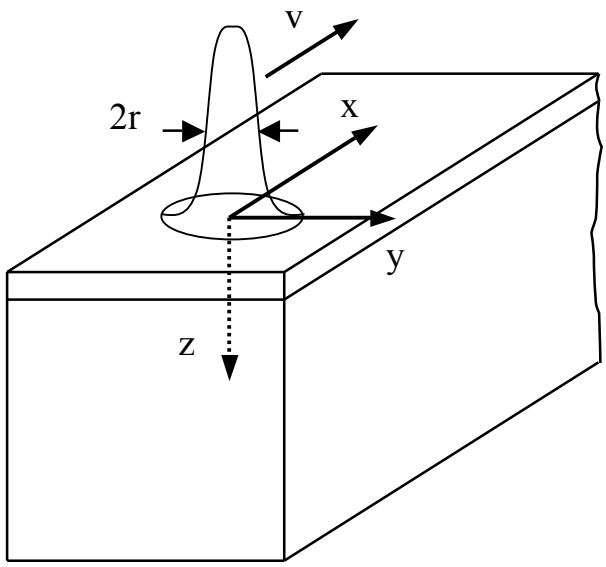


*Figure 6: Schematic illustration of laser annealing geometry.*

Once the temperature distribution in the NiTi film is known, a criterion is needed to determine where the film has crystallized. This criterion is based on the results of a kinetics study of the crystallization process [11] and takes into account both temperature and dwell time. After a time $t$, the fraction of NiTi that has transformed at a given location is equal to [13-16]

$$f(t) = 1 - \exp\left( -\frac{4}{3}\pi \int_0^t I(T(\tau)) \left[ \int_\tau^t u(T(\xi)) d\xi \right]^3 d\tau \right). \qquad (2)$$

In this expression, $I$ and $u$ are the temperature-dependent nucleation and growth rates of the

crystallites, and $T(t)$ is the temperature history of the location under consideration. Figure 7 shows typical temperature profiles obtained from the FEM simulations if the center of the laser beam is swept across a point. Using Eq. (2) and the FEM

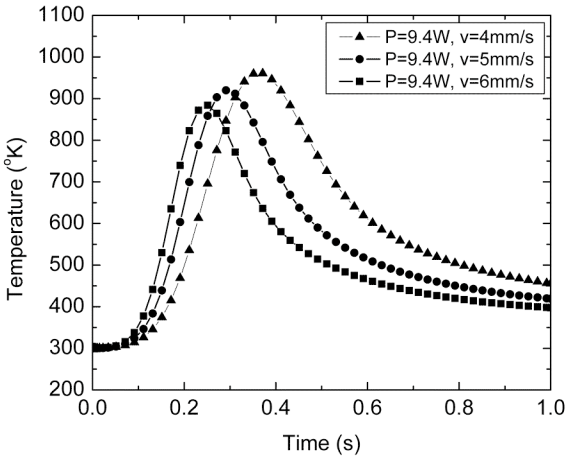


*Figure 7: Temperature profile at the center of the laser beam for various scan velocities and fixed laser power.*

temperature profiles, the transformed fraction can be calculated as a function of location. The width of the crystallized region is then determined by setting the transformed fraction equal to a constant value (0.99 in this case). From the temperature profiles, one can then determine an equivalent crystallization temperature, $T_e$. This equivalent temperature varies with laser scan speed as illustrated in Figure 8. Evidently, $T_e$ follows an Arrhenius-type relationship

$$v = v_o \exp\left(-\frac{Q}{kT_e}\right) \tag{3}$$

where $Q$ is equal to 3.65 ± 0.1 eV, approximately the same as the crystallization activation energy in reference [11]. At typical laser dwell times, the crystallization temperature is approximately 840 K.

One additional piece of information is required before quantitative predictions can be made with regards to the extent of crystallization, i.e., the value of the coefficient of reflection in Eq. (1). The reflection coefficient of the air-NiTi surface for a wavelength 925nm was measured to be 0.65 at room temperature [9]. Figure 9 shows the width of the crystalline regions as a function of laser power density and scan velocity as obtained from the FEM simulations using an R of 0.65. From a comparison of Figures 3 and 9, it is evident that the FEM simulations systematically overestimate the power needed for a given crystallization width. This is caused by the oxide layer that forms on top of the

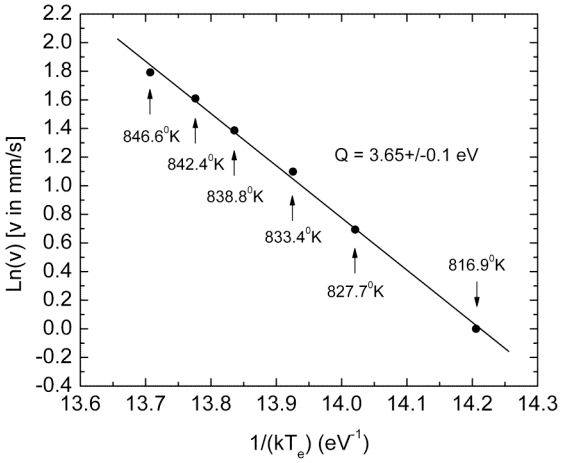


*Figure 8: Equivalent crystallization temperature for different scan speed.*

NiTi film during the laser annealing process [9]. The oxide layer increases the absorption of laser power because the reflectivity of the NiTi film decreases with increasing oxide thickness. In order to account for this effect, the reflectivity was used as a fitting parameter to obtain good agreement between Figures 3 and 9. At the same time, the oxide thickness of the laser annealed specimens was determined as described in reference [9]. Figure 10 shows the reflectivity as a function of oxide

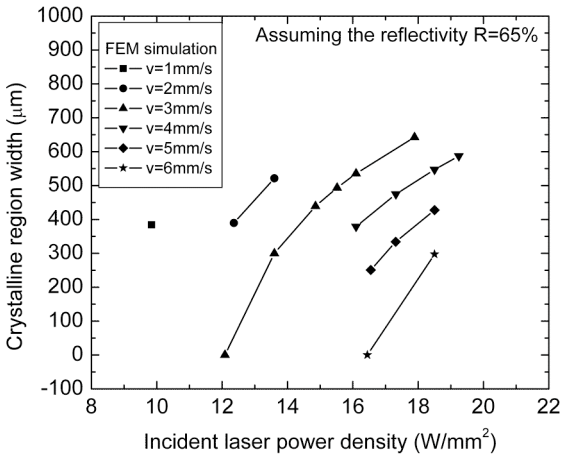


*Figure 9: Width of crystallized regions according to FEM simulations as a function of laser power density and scan velocity.*

thickness, along with data obtained from furnace annealed NiTi films. It is clear that the reflectivity values obtained through fitting are in good agreement with the reflectivity of the furnace-grown oxide. The figure shows that the oxide thickness after laser-annealing is approximately 75 nm. The experimental results along with the simulations show that it is critical to reduce oxide growth during the laser-annealing process: The reflectivity of the coating decreases rapidly as the oxide thickness increases, making the annealing process more difficult to control and to simulate. Furthermore,

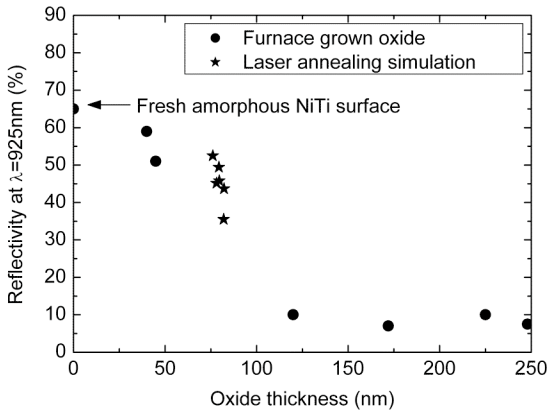


*Figure 10: The reflectivity as a function of oxide thickness.*

oxidation results in a Ni-rich layer below the oxide with a slightly different martensite start temperature. Oxide formation can of course be minimized by performing the laser annealing experiments in vacuum or an inert atmosphere. Alternately, it may be possible to protect the NiTi with a thin inert coating such as silicon nitride. This technique has the advantage that the reflectivity can be fine-tuned through a judicious choice of the nitride thickness and that the annealing process can be performed under ambient conditions.

## Conclusions

We have presented the results of a crystallization study on NiTi shape memory thin films in which amorphous films were annealed by scanning a laser across the surface of the film. Our results show that under the correct conditions of laser power density and scanning speed, it is indeed possible to crystallize the films. Moreover, X-ray diffraction clearly shows the formation of martensite in the crystallized sections of the film. The temperature profiles induced by the laser beam were calculated using a three-dimensional finite element model. The model takes into account the crystallization kinetics of amorphous NiTi and allows prediction of the size of the crystallized regions as a function of laser annealing parameters if the reflectivity of the NiTi surface is known. Our results further show that it is critical to minimize oxide growth during the laser-annealing process for good control of the process.

## References


[1] Busch, J.D. *et al*, "Shape-memory Properties in Ni-Ti Sputter-deposited Film," *J Appl Phys*, Vol. 68, (1990), pp. 6224-6228.

[2] Walker, J.A. *et al*, "Thin-film Processing of TiNi Shape Memory Alloy," *Sensors and Actuators A*, Vol. 21-23, (1990), pp. 243-246.

[3] Ishida, A. *et al*, "Shape Memory Thin Films of Ti-Ni Formed by Sputtering," *Thin Solid Films*, Vol. 228, (1993), pp. 210-214.

[4] Wolf, R.H. and Heuer, A.H., "TiNi(Shape memory) Films on Silicon for MEMS application," *J Microelectromech Syst*, Vol. 4, (1995), pp. 206-212.

[5] Miyazaki S. and Ishida A., "Martensitic Transformation and Shape Memory Behavior in Sputter-deposited TiNi-base Thin Films," *Mater Sci Eng A*, Vol. 273-275, (1999), pp. 106-133.

[6] Grummon, D.S. *et al*, "Progress on Sputter-deposited Thermotractive Titanium-nickel Films," *J. Phys. IV*, Vol. 5, No. C8, (1995), pp. 665-670.

[7] Shih, C.L. *et al*, "A Robust Co-sputtering Fabrication Procedure for TiNi Shape Memory Alloys for MEMS" *J Microelectromech Syst*, Vol. 10, (2001), pp. 69-79.

[8] Bellouard, Y. *et al*, "Local Annealing of Complex Mechanical Devices: A New Approach for Developing Monilithic Micro-devices" *Mater Sci Eng A*, Vol. 273-275, (1999), pp. 795-798.

[9] Khelfaoui, F. et al., "An investigation of the oxidation of laser and furnace-annealed sputter-deposited NiTi films using reflectivity measurement" Proc SMST-2004, Germany, 2004.

[10] Touloukian Y. S. et al., Thermophysical Properties of Matter, IFI/Plenum (New York, 1970).
[11] Wang, X. and Vlassak, J.J., "Crystallization Kinetics of Amorphous NiTi Shape Memory Alloy Thin Films," *Scripta Materialia*, Vol. 54, (2006), pp. 925-930.
[12] Wang X., Bellouard Y., and Vlassak J.J., "Laser Annealing of Amorphous NiTi Shape Memory Alloy Thin Films to Locally Induce Shape Memory Properties", *Acta Materialia*, Vol. 53, (2005), pp. 4955-4961.
[13] Christian, J.W. The theory of transformation in metals and alloys, 2nd ed. Pergamon, (New York, 1975).
[14] Avrami M., "Kinetics of Phase Change. I General Theory," *J Chem Phys*, Vol. 7, (1939), pp. 1103-1112.
[15] Avrami M. "Kinetics of Phase Change. II Transformation-Time Relations for Random Distribution of Nuclei," *J Chem Phys*, Vol. 8, (1940), pp. 212-224.
[16] Avrami M. "Kinetics of Phase Change. III Granulation, Phase Change, and Microstruture," *J Chem Phys*, Vol. 9, (1941), pp. 177-184.